Results on Tensor Product-based Model Transformation of Magnetic Levitation Systems

Elena-Lorena Hedrea, Radu-Emil Precup, Claudia-Adina Bojan-Dragos

Department of Automation and Applied Informatics, Politehnica University of Timisoara, Bd. V. Parvan 2, RO-300223 Timisoara, Romania
E-mail: elena.constantin@student.upt.ro, radu.precup@upt.ro, claudia.dragos@upt.ro

Abstract: In this paper the TP-based model transformation method is used in order to obtain a Tensor Product-based model of magnetic levitation systems which approximates the behavior of the plant, but exhibiting a numerical approximation error. In order to test the derived TP model, the behavior of the TP model is compared to the laboratory equipment behavior taking into consideration five testing scenarios. Experimental results show that approximation errors are generally low, but depend on model parameters.

Keywords: LTI systems; qLPV models; Tensor Product; magnetic levitation systems; transformation spaces

1 Introduction

The Tensor Product-based Model transformation (TPM) technique is a numerical, non-heuristic method that is capable of transforming a dynamic system model, given over a bounded domain, into parameter-varying weighted combination of parameter independent (constant) system models under the form of Linear Time-Invariant (LTI) systems. More precisely the TPM starts with Linear Parameter–Varying (LPV) dynamic models and derivates Linear Time-Invariant (LTI) systems as shown, for example, in the seminal papers and book (Baranyi, 2004) [1], (Petres et al., 2007) [2] and (Baranyi et al., 2013) [3].

TPM has the advantage of allowing linear matrix inequality (LMI) and parallel distributed compensation (PDC) frameworks to be applied immediately to the resulting affine models. This leads to tractable and improved control system performance.

The derivations of TP-based model transformation design approaches for different application plants such as models of diabetes mellitus and nonlinear insulin-glucose dynamics, a nonlinear flexible joint robot system, a multi-tank system, etc., are given in the specialized literature in (Korondi, 2006) [4], (Galambos et al., 2015) [5] and (Hedrea et al., 2018) [6]. The combination with Proportional–Integral–Derivative controller tuning is treated in (Kuti and Galambos, 2018) [7]. The book (Baranyi, 2016) [8] and the papers (Szöllösi and Baranyi, 2016) [9] and (Szöllösi and Baranyi, 2016) [10] are important as they prove that the manipulation of the TPM is neccesary in control deisgn like PDC. The latest results where the number of variables or inputs may differ are presented in (Baranyi, 2018) [11], and also in (Baranyi, 2019) [12] if the TPmodel starts from $\mathbf{f}(\mathbf{x}, \mathbf{u}, \mathbf{p})$, where the matrix structure is unknown.

The Magnetic Levitation System (MLS) is a laboratory equipment (LabEq) used for experiments. It is an important benchmark to test linear and nonlinear modeling and control approaches applied to various areas including transportation systems. Some recent modeling solutions proposed for MLS include neural networks reported in (Rubio et al., 2017) [13], evolving fuzzy models reported in (Precup et al., 2017) [14] and Euler–Lagrange method reported in (Sun et al., 2017) [15]. The evolving fuzzy models prove to be popular recently and the results related to MLS can be considered as belonging to the hot fields of transportation systems and automotive technology as exemplified by Precup et al. (2017) in [16].

This paper is an extended version of the paper (Hedrea et al., 2019) [17], where the derivation of a TP–based model (TPmodel) using TPM was recently proposed. The TPmodel is then tested and its validation is improved using two testing scenarios. The topic at hand should be of interest to many engineers hoping to apply the TPmodel as a numerical modeling approach. The main contributions of this paper, which required restructuring in all sections including authors team, are pointed out as follows: the authors use the same main steps as the ones presented in [17] in order to obtain the TPmodel of the stabilized reduced order linearized model of a magnetic levitation system (referred to as stMaglev) and discussed in (Inteco, 2008) [18] and (Bojan-Dragos et al., 2018) [19]. However, the derived model is tested using four new testing scenarios. More precisely four control inputs (signals), namely a staircase control input, a sine control input, a chirp control input and a Pulse–Width modulation (PWM) control input, were applied to both stMaglev LabEq and TPmodel of stMaglev and their corresponding outputs were compared.

A part of the results given in both [17] and the current paper represent a sample of the continuation of the fruitful cooperation with the team of the Óbuda University (Budapest, Hungary). The excellent scientific contributions and management activity of Prof. Imre J. Rudas are kindly acknowledged. Some representative well-accepted joint papers in this regard are given in (Pozna et al., 2010 [20], (Haidegger et al., 2012) [21], (Precup et al., 2012) [22] and (Takács et al., 2015) [23].

The paper treats these topics: Section 2 gives the steps of TPM and the derivation of the TPmodel for stMaglev. Section 3 illustrates the four testing scenarios used for testing the derived TPmodel for stMaglev and Section 4 highlights the conclusions.

2 The TPmodel Derivation for stMaglev

2.1 TP-based Model Design Approach

When creating TPmodels for system representations, it is always useful for the reader to understand the base system equations of the physical system, preferably in a continuous–time state–space representation. That is the reason why such details are given in the section.

The TP-based model transformation is a numerical non-heuristic method which was first introduced by Baranyi (2004) in [1]. This method uses the high order singular value decomposition (HOSVD) technique in order to generate convex polytopic forms starting with the LPV models. In order to derivate a TPmodel uring the TPM technique the six steps with the diagram illustrated by Hedrea et al. (2019) in [17] and detailed in the following paragraphs are used.

In the first step the Transformation Space (TSp) is defined. Let $\mathbf{p}=[p_1\ \ p_2 \dots p_n]^T \in \mathbf{\Omega}$ be a parameter vector and n the number of parameters. Therefore, $\mathbf{\Omega}=[a_1,b_1]\times[a_2,b_2]\times\dots\times[a_n,b_n]\subset\Re^n$ is the TSp with the bounds of the intervals $[a_i,b_i]$, i = 1...n chosen according to the plant specifications. A TSp $\mathbf{\Omega}=[a_1,b_1]\times[a_2,b_2]$ for two parameters is illustrated in (Hedrea et al., 2019) [17].

In the second step the Dicretization Grid (DG) is defined. Let $M_i, M_i \in \mathbf{N}, M_i \geq 2$ be the number of the discretization points from each interval [a_i, b_i], i = 1...n, including the ends of the intervals, which are computed using the technique described in (Baranyi et al., 2013) [3]. Therefore, the DG is given as:

$$\begin{aligned}&\mathbf{M}=\{\mathbf{g}_{m_1,m_2,\dots,m_n}\in\mathbf{\Omega}\},\ m_i=1\dots M_i,\ i=1\dots n,\\&|\mathbf{M}|=M_1\cdot M_2\cdot\ldots\cdot M_n,\end{aligned} \tag{1}$$

where $\mathbf{g}_{m_1,m_2,\dots,m_n}\in\mathbf{\Omega}$ is a discretization point. An example of DG with $|\mathbf{M}|=M_1\cdot M_2=8\cdot 6$, where n = 2, for M_1 = 8 and M_2 = 6 is given in (Hedrea et al., 2019) [17].

In the third step the discretized Tensor (dTens) is determined. Using the LPV model of the plant as shown in (Baranyi et al., 2013) [3] and (Hedrea et al., 2018) [6], the System matrix (Sm) can be defined as:

$$\mathbf{S}(\mathbf{p}) = \begin{bmatrix} \mathbf{A}(\mathbf{p}) & \mathbf{B}(\mathbf{p}) \\ \mathbf{C}(\mathbf{p}) & \mathbf{D}(\mathbf{p}) \end{bmatrix} \in \Re^{(l+q)\times(m+q)}, \quad \mathbf{S}(\mathbf{p}) = [s_{ij}(\mathbf{p})]_{i=1...(l+q),\, j=1...(m+q)}. \tag{2}$$

Considering the parameter vector equal to the discretization point $\mathbf{p} = \mathbf{g}_{m_1,m_2,...,m_n} = [g_{1,m_1} \quad g_{2,m_2} \quad \dots \quad g_{n,m_n}]^T \in \mathbf{M}$ the Discretized System matrix (DSm) is given as:

$$\mathbf{S}^D_{m_1,m_2,...m_n} = \mathbf{S}(\mathbf{g}_{m_1,m_2,...m_n}) \in \Re^{(l+q)\times(m+q)}, \quad \mathbf{S}^D_{m_1,m_2,...m_n} = [s_{ij}(\mathbf{g}_{m_1,m_2,...m_n})]_{i=1...(l+q),\, j=1...(m+q)} \tag{3}$$

and the dTens $\mathbf{S}^D$ is defined as:

$$\mathbf{S}^D = [\mathbf{S}^D_{m_1,m_2,...m_n}]_{m_1=1...M_1, m_2=1...M_2,...,m_n=1...M_n} \in \Re^{M_1\times M_2\times..\times M_n\times(l+q)\times(m+q)}. \tag{4}$$

A particular example of a dTens computed for two parameters $p_1 \in [a_1, b_1]$ and $p_2 \in [a_2, b_2]$ with the TSp $\mathbf{\Omega} = [a_1, b_1] \times [a_2, b_2]$ and the DG $|\mathbf{M}| = M_1 \cdot M_2 = 8 \cdot 6$ has the following expression:

$$\mathbf{S}^D = \begin{bmatrix} \mathbf{S}^D_{1,1} & \mathbf{S}^D_{1,2} & \dots & \mathbf{S}^D_{1,6} \\ \mathbf{S}^D_{2,1} & \mathbf{S}^D_{2,2} & \dots & \mathbf{S}^D_{2,6} \\ \dots & \dots & \dots & \dots \\ \mathbf{S}^D_{8,1} & \mathbf{S}^D_{8,2} & \dots & \mathbf{S}^D_{8,6} \end{bmatrix} \in \Re^{8\times 6\times(l+q)\times(m+q)}. \tag{5}$$

In the fourth step the HOSVD is applied in order to obtain the singular values of the dTens $\mathbf{S}^D \in \mathbf{R}^{M_1\times M_2\times..\times M_n\times(l+q)\times(m+q)}$, which can be expressed as $\mathbf{S}^D = \mathbf{S} \overset{N}{\underset{n=1}{\otimes}} \mathbf{U}_n$ (Baranyi et al., 2013) [3] where $\mathbf{U}_n$, $\mathbf{S}$ and $\otimes$ are expressed in (Baranyi et al., 2013) [3] and (Hedrea et al., 2019) [17].

The n–mode matrix $\mathbf{S}^D_{(n)} \in \Re^{M_n\times(M_{n+1}M_{n+2}...(m+q)M_1M_2...(l+q))}$ can be given as $\mathbf{S}^D_{(n)} = [\mathbf{s}^D_r]$, where $\mathbf{s}^D_r \in \Re^{M_n}$ denote the column vectors of the M_n dimension of tensor $\mathbf{S}^D$ and r = 1...R, with $R = M_{n+1}M_{n+2}...(m+q)M_1M_2...(l+q)$.

In order to compute the HOSVD of the tensor $\mathbf{S}^D$ n singular value decompositions (SVD) made for all the n–mode matrices $\mathbf{S}^D_{(n)}$ are made using the theorem given in (Hedrea et al., 2019) [17] and (Lathauwer et al., 2000) [25], whose proof is given by Lathauwer et al. (2000) in [25].

Using this theorem given in (Lathauwer et al., 2000) [25], the SVD (with the three steps a), b) and c) detailed in [16]) of the *n*–mode matrix $\mathbf{S}_{(n)}^{D}$ can be given as $\mathbf{S}_{(n)}^{D} = \mathbf{U}_n \mathbf{\Sigma}_n \mathbf{V}_n^T$ (Hedrea et al., 2019) [17].

Finally the matrices $\mathbf{U}_n$ and $\mathbf{V}_n$ are computed following the steps taken from (Hedrea et al., 2019) [17].

In the fifth step the numerical values of the weighting functions are determined. The column vectors $\mathbf{u}_{n,I_n}$ in the matrix $\mathbf{U}_n$ are called weighting vectors and they contain the values of the w.f. $\mathbf{w}_n(\mathbf{p}_{m_1,m_2,..m_n})$ for $\mathbf{p}_{m_1,m_2,..m_n} = (g_{1,m_1},\cdots g_{n,m_n})$ (Baranyi et al., 2013) [3]:

$$\mathbf{w}_n(\mathbf{p}_{m_1,m_2,..m_n}) = \mathbf{u}_{n,I_n}. \tag{6}$$

In the final step the core tensor $\mathbf{S}_f$ is computed using the dTens $\mathbf{S}^D$ and the matrix $\mathbf{U}_N$ from the above steps (Baranyi et al., 2013) [3]:

$$\mathbf{S}_f = \mathbf{S}^D \overset{N}{\underset{n=1}{\otimes}} \mathbf{U}_N^T \tag{7}$$

The core tensor $\mathbf{S}_f$ is defined as $\mathbf{S}_f = \sum_{m_1=1}^{M_1}\sum_{m_2=1}^{M_2}\cdots\sum_{m_n=1}^{M_n}\prod_{n=1}^{N}\mathbf{w}_n(\mathbf{p}_{m_1,m_2,..m_n})\mathbf{S}_{m_1,m_2,...m_n}^{LTI}$ with the equivalent notation $\mathbf{S}(\mathbf{p}(t)) = \mathbf{S}_f \otimes \mathbf{w}_n(\mathbf{p}_{m_1,m_2,..m_n})$ presented in (Baranyi, 2004) [1].

2.2 Derivation of TPmodel for stMaglev

The modelled plant considered in this paper is a laboratory system based on the magnetic levitation principle, which includes a metallic frame with one upper electromagnet, Electromagnet1, and one lower electromagnet, Electromagnet2, between which a ferromagnetic sphere levitates as shown in Figure 1. The position of the ferromagnetic sphere is measured using position sensors. In order to ensure the communication between the hardware and the software components one computer interface is used.

The base system equations for MLS are (Inteco, 2008) [18]:

$$\begin{aligned}
&\dot{x}_1(t) = v(t),\\
&\dot{v}(t) = -\frac{i_{EM1}^2(t)\cdot F_{emP1}\cdot \exp[-x_1(t)/F_{emP2}]}{m\cdot F_{emP2}} + g\\
&\qquad + \frac{i_{EM2}^2(t)\cdot F_{emP1}\cdot \exp[-(x_d - x_1(t))]/F_{emP2}}{m\cdot F_{emP2}},\\
&\dot{i}_{EM1}(t) = \frac{k_i\cdot u_{EM1}(t)+c_i - i_{EM1}(t)}{(f_{iP1}/f_{iP2})\cdot \exp[-x_1(t)/f_{iP2}]},\\
&\dot{i}_{EM2}(t) = \frac{k_i\cdot u_{EM2}(t)+c_i - i_{EM2}(t)}{(f_{iP1}/f_{iP2})\cdot \exp[-(x_d - x_1(t))/f_{iP2}]},\\
&y(t) = k_m\cdot x_1(t),
\end{aligned} \tag{8}$$

where the ferromagnetic sphere position (m) is $x_1 \in [0, 0.0016]$, the speed of the ferromagnetic sphere (m/s) is $v\in\Re$, the current of Electromagnet1 (A) is $i_{EM1}\in[0.03884, 2.38]$, the current of Electromagnet2 (A) is $i_{EM2}\in[0.03884, 2.38]$, the control signals applied to Electromagnet1 and Electromagnet2, respectively (V) are $u_{EM1}\in[0.005, 1]$ and $u_{EM2}\in[0.005, 1]$ and the measured output of the process (m) is denoted by y. The process parameters are: m=0.0571 [kg] – the mass of ferromagnetic sphere, $F_{emP1}=1.7521\cdot 10^{-2}$ [H], $F_{emP2}=5.8231\cdot 10^{-3}$ [m], k_i=0.0243 [A], c_i=2.5165 [A], $f_{iP1}=1.4142\cdot 10^{-4}$ [ms], $f_{iP2}=4.5626\cdot 10^{-3}$ [m] (Bojan-Dragos et al., 2018) [19].

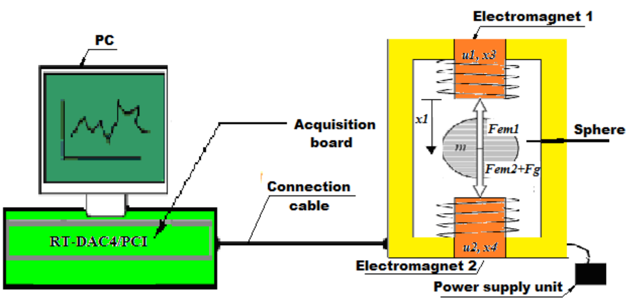

Figure 1
Experimental setup for MLS

In order to determine the qLPV model of the process, which is later used in the derivation of the TPmodel a stabilizing control solution was designed (Bojan-Dragos et al., 2018) [19] resulting the stabilized linearized model for MLS (stMaglev):

Therefore, the qLPV model representation of stMaglev is expressed as

$$\begin{aligned}&\dot{\mathbf{x}} = \mathbf{A}_x(\mathbf{p})\mathbf{x} + \mathbf{b}_{1x}(\mathbf{p})u_{1x},\\ &y = \mathbf{c}^T(\mathbf{p})\mathbf{x},\\ &\mathbf{x} = [x_1 \quad v \quad i_{EM1}]^T,\ \mathbf{p} = [x_1 \quad i_{EM1}]^T,\end{aligned} \tag{9}$$

where the matrices $\mathbf{A}_x(\mathbf{p})$, $\mathbf{b}_{1x}(\mathbf{p})$ and $\mathbf{c}^T(\mathbf{p})$ are (Bojan-Dragos et al., 2018) [19]

$$\mathbf{A}_x(\mathbf{p}) = \begin{bmatrix} 0 & 1 & 0 \\ a_{21}(\mathbf{p}) & 0 & a_{23}(\mathbf{p}) \\ a_{31}(\mathbf{p}) & a_{32}(\mathbf{p}) & a_{33}(\mathbf{p}) \end{bmatrix},\ \mathbf{b}_{1x}(\mathbf{p}) = \begin{bmatrix} 0 \\ 0 \\ b_{31}(\mathbf{p}) \end{bmatrix}, \mathbf{c}^T(\mathbf{p}) = [1\ 0\ 0], \tag{10}$$
$$\mathbf{A}_x(\mathbf{p}) \in \Re^{3x3},\ \mathbf{b}_{1x}(\mathbf{p}) \in \Re^{3x1},\ \mathbf{c}^T(\mathbf{p}) \in \Re^{1x3},\ u_{1x} \in \Re,$$

with the elements:

$$\begin{aligned}&a_{21}(\mathbf{p}) = \frac{\mathbf{p}(2)^2}{m}\frac{F_{emP1}}{F_{emP2}^2}e^{-\frac{\mathbf{p}(1)}{F_{emP2}}},\ a_{23}(\mathbf{p}) = -\frac{2\mathbf{p}(2)}{m}\frac{F_{emP1}}{F_{emP2}}e^{-\frac{\mathbf{p}(1)}{F_{emP2}}},\\ &a_{31}(\mathbf{p}) = -(k_i u_{1x} + c_i - \mathbf{p}(2))\frac{\mathbf{p}(1)}{f_{iP1}} \cdot e^{\frac{\mathbf{p}(1)}{f_{iP2}}} + 66.33 \cdot k_i \cdot \frac{f_{iP2}}{f_{iP1}} \cdot e^{\frac{\mathbf{p}(1)}{f_{iP2}}},\\ &a_{32}(\mathbf{p}) = 1.62 \cdot k_i \cdot \frac{f_{iP2}}{f_{iP1}} \cdot e^{\frac{\mathbf{p}(1)}{f_{iP2}}}, a_{33}(\mathbf{p}) = -\frac{f_{iP2}}{f_{iP1}} \cdot e^{\frac{\mathbf{p}(1)}{f_{iP2}}} - 0.15 \cdot k_i \cdot \frac{f_{iP2}}{f_{iP1}} \cdot e^{\frac{\mathbf{p}(1)}{f_{iP2}}},\\ &b_{31}(\mathbf{p}) = k_i \cdot \frac{f_{iP2}}{f_{iP1}} \cdot e^{\frac{\mathbf{p}(1)}{f_{iP2}}}.\end{aligned} \tag{11}$$

where $\mathbf{p}$ is vector of the parameters which contains the state variable $\mathbf{p}(1)$ – the position of the ferromagnetic sphere and the state variable $\mathbf{p}(2)$ – the top electromagnet current, v is the speed of the ferromagnetic sphere, u_{1x} is the plant input, y is the measured output of the process.

Introducing in (9) the Sm $\mathbf{S}(\mathbf{p}) = [\mathbf{A}_x(\mathbf{p}) \quad \mathbf{b}_{1x}(\mathbf{p})] \in \Re^{3\times 4}$, the model is transformed in the qLPV state–space form

$$\begin{aligned}&\dot{\mathbf{x}} = \mathbf{S}(\mathbf{p})[\mathbf{x}^T \quad u_{1x}]^T,\\ &y = \mathbf{c}^T(\mathbf{p})\mathbf{x}.\end{aligned} \tag{12}$$

with the following LTI models (Hedrea et al., 2017) [26]:

$$\begin{aligned}\dot{\mathbf{x}} &= \mathbf{S}(\mathbf{p}) \bigotimes_{n=1}^{N} \mathbf{w}_n(\mathbf{p}_n)[\mathbf{x}^T \quad u_{1x}]^T\\ &= \sum_{m_1=1}^{M_1}\sum_{m_2=1}^{M_2} w_{1,m_1}(p_1) w_{2,m_2}(p_2)\mathbf{S}_{m_1,m_2}[\mathbf{x}^T \quad u_{1x}]^T,\\ y &= \mathbf{c}^T(\mathbf{p})\mathbf{x},\end{aligned} \tag{13}$$

The LTI Sms contain the matrices $\mathbf{A}_{x_{m_1,m_2}}$ and $\mathbf{b}_{1x_{m_1,m_2}}$ from the state–space model

$$\dot{\mathbf{x}} = \sum_{m_1=1}^{3}\sum_{m_2=1}^{3} w_{1,m_1}(p_1)w_{2,m_2}(p_2)(\mathbf{A}_{x_{m_1,m_2}}\mathbf{x} + \mathbf{b}_{1x_{m_1,m_2}}u_{1x}),$$
$$y = \mathbf{c}^T(\mathbf{p})\mathbf{x}, \tag{14}$$

3 Experimental Results

Using the TP Tool, with its operation mode described by Nagy et al. (2007) in [27], the matrices $\mathbf{S}_{m1,m2}$ obtained for stMaglev are given in (14) and the w.f.s are presented in Figure 2 for the two parameters, namely the sphere position and the top electromagnetic current.

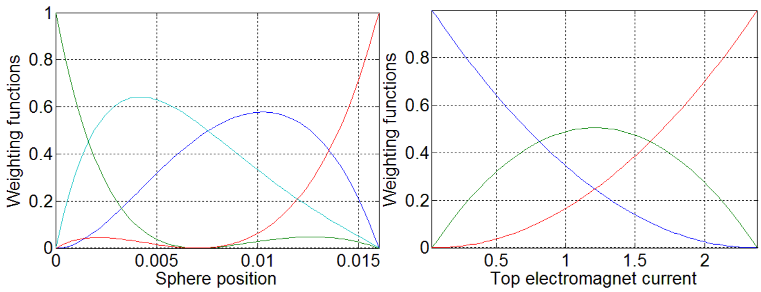

Figure 2

W.f.s obtained by TPM of stMaglev (sphere position and top electromagnetic current)

$$
\begin{aligned}
&\mathrm{S}_{1,1}=\left[\begin{array}{ccc|c} 0 & 1 & 0 & 0 \\ 709.3 & -0.1 & -60.7 & 0 \\ -3413.2 & -248.6 & 84 & -153.5 \end{array}\right],\ \mathrm{S}_{2,1}=\left[\begin{array}{ccc|c} 0 & 1 & 0 & 0 \\ 157 & -0.1 & -8 & 0 \\ 60074 & 4385 & -1482 & 2707 \end{array}\right],\\
&\mathrm{S}_{3,1}=\left[\begin{array}{ccc|c} 0 & 1 & 0 & 0 \\ 1411.7 & -0.1 & -127.5 & 0 \\ 1795.1 & 131.5 & -44.4 & 81.2 \end{array}\right],\ \mathrm{S}_{4,1}=\left[\begin{array}{ccc|c} 0 & 1 & 0 & 0 \\ -183 & -0.1 & 24 & 0 \\ 36927 & 2699 & -912 & 1666 \end{array}\right],\\
&\mathrm{S}_{1,2}=\left[\begin{array}{ccc|c} 0 & 1 & 0 & 0 \\ 76.5 & -0.1 & -2 & 0 \\ -3282.4 & -248.6 & 84 & -153.5 \end{array}\right],\ \mathrm{S}_{2,2}=\left[\begin{array}{ccc|c} 0 & 1 & 0 & 0 \\ 72 & -0.1 & -8 & 0 \\ 58602 & 4385 & -1482 & 2707 \end{array}\right],\\
&\mathrm{S}_{3,2}=\left[\begin{array}{ccc|c} 0 & 1 & 0 & 0 \\ 83.8 & -0.1 & -4.1 & 0 \\ 1795.1 & 131.5 & -44.4 & 81.2 \end{array}\right],\ \mathrm{S}_{4,2}=\left[\begin{array}{ccc|c} 0 & 1 & 0 & 0 \\ -68 & -0.1 & 1 & 0 \\ 36305 & 2699 & -912 & 1666 \end{array}\right],\\
&\mathrm{S}_{1,3}=\left[\begin{array}{ccc|c} 0 & 1 & 0 & 0 \\ 24496 & -0.1 & -120 & 0 \\ -3544 & -249 & 84 & -153.5 \end{array}\right],\ \mathrm{S}_{2,3}=\left[\begin{array}{ccc|c} 0 & 1 & 0 & 0 \\ 3356 & -0.1 & -16 & 0 \\ 61546 & 4385 & -1482 & 2707 \end{array}\right],\\
&\mathrm{S}_{3,3}=\left[\begin{array}{ccc|c} 0 & 1 & 0 & 0 \\ 51329 & -0.1 & -251 & 0 \\ 1795 & 132 & -44 & 81.2 \end{array}\right],\ \mathrm{S}_{4,3}=\left[\begin{array}{ccc|c} 0 & 1 & 0 & 0 \\ -9650 & -0.1 & 48 & 0 \\ 37549 & 2699 & -912 & 1666 \end{array}\right]
\end{aligned}
\tag{15}
$$

In order to test the derived TPmodel, five testing scenarios are presented in this extented paper and are detailed in the followings. The same testing signal was applied both to the stMaglev LabEq and to the TPmodel derived for stMaglev on the time frame of 20 s and their corresponding outputs, y_{MLS_j} and y_{TP_j}, $j \in \{PRBS$, *STAIRS*, *SINE*, *CHIRP*, $PWM\}$, were compared (Figure 3). The initial state vector matching the experiments was $\mathbf{x}_0 = [0.0083 \quad 0 \quad 0]^T$.

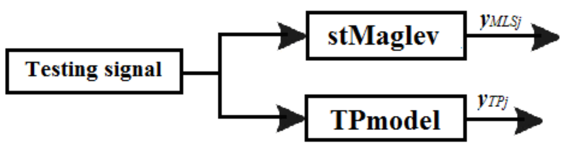

Figure 3
Testing block diagram for stMaglev LabEq and TPmodel

The first testing scenario is the same as the first one used by Hedrea et al. (2019) in [17] and consists in applying a Pseudo Random Binary Signal (PRBS) with a 0.008 m amplitude as control input with the corresponding plot of the sphere position versus time illustrated in Figure 4.

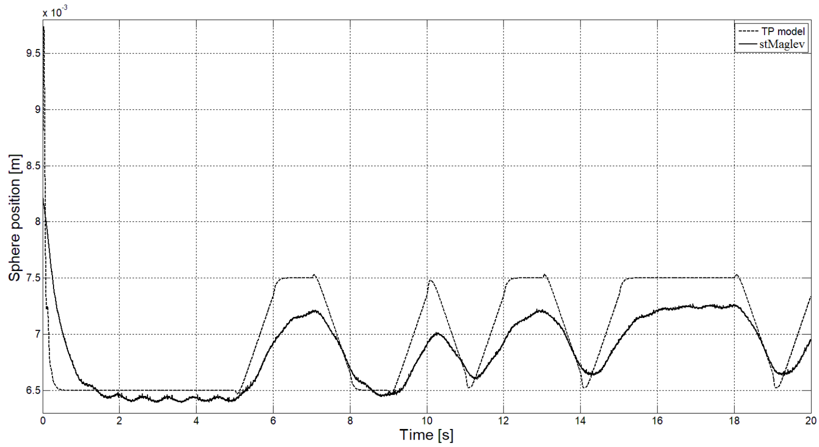

Figure 4
The time response of TPmodel and stMaglev with PRBS control input

The next four testing scenarios consist in applying four new control inputs (signals), namely a staircase control input, a sine control input, a chirp control input and a PWM control input, to both stMaglev LabEq and TPmodel of stMaglev.

In the first new testing scenario, the plot of the sphere position versus time obtained after applying a staircase control input with a $R1$=0.006 m, $R2$=0.008 m and $R3$=0.007 m amplitude as control input is illustrated in Figure 5.

In the second new testing scenario, the plot of the sphere position versus time obtained after applying a sine control input with a 0.001 m amplitude as control input is illustrated in Figure 6.

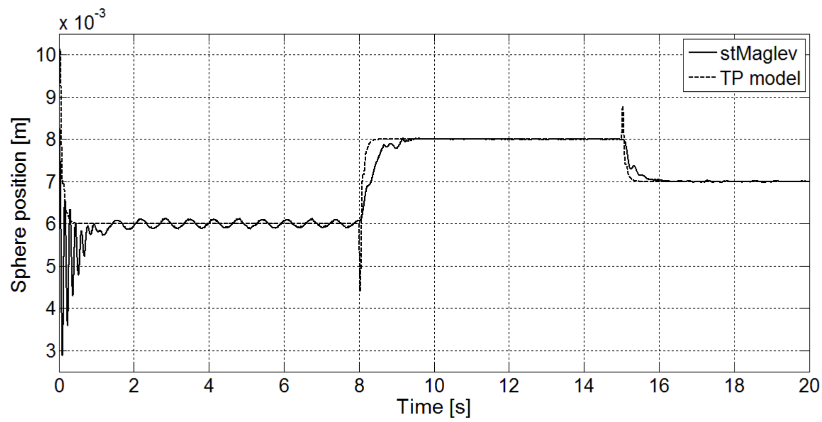

Figure 5
The time response of TPmodel and stMaglev with PRBS control input

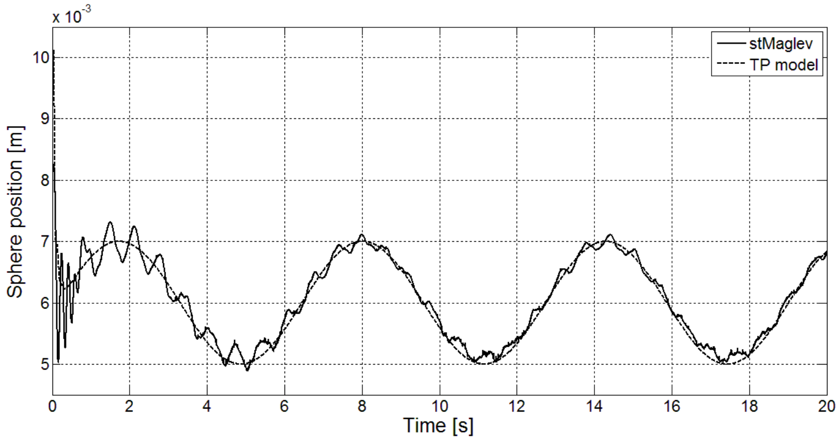

Figure 6

The time response of TPmodeland stMaglev with sine control input

In the third testing scenario the plot of the sphere position versus time obtained after applying a Chirp control input with a 0.1 initial frequency as control input is illustrated in Figure 7.

In the fourth testing scenario the plot of the sphere position versus time obtained after applying a Pulse–width modulation (PWM) control signal with a 0.0012 m amplitude, a 50% pulse width as control input is illustrated in Figure 8.

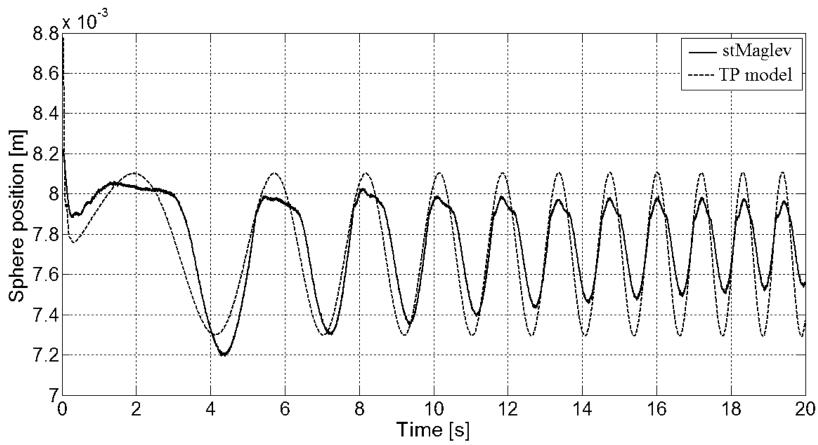

Figure 7

The time response of TPmodel and stMaglev with chirp control input

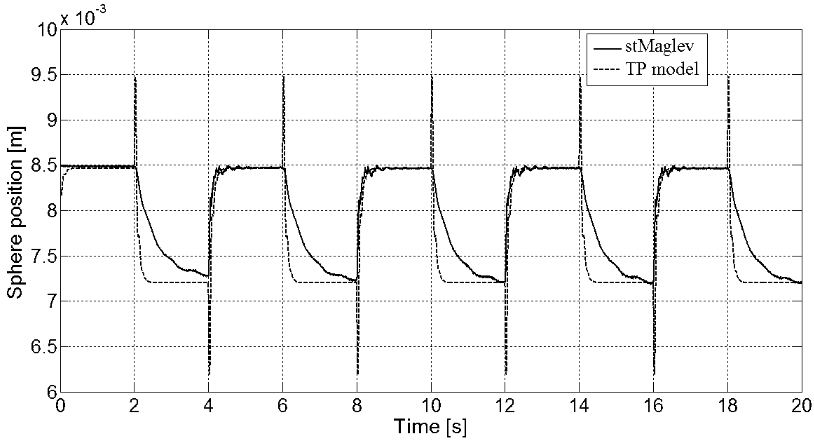

Figure 8
The time response of TPmodel and stMaglev with PWM control input

In order to better highlight the performances of the TPmodel derived for stMaglev in all testing scenarios the following performance indices were computed: the modeling errors, the mean square error and the percent relative modeling error.

The modeling errors were computed as the difference between the output responses of the real–world stMaglev (experimenting on the LabEq) and the TPmodel of stMaglev:

$$e_j = y_{MLS_j} - y_{TP_j}, \tag{16}$$

The mean square error (MSE) was also calculated as:

$$\mathrm{MSE}_j = \frac{1}{N}\sum_{t_d=1}^{N}(e_j(t_d))^2, \tag{17}$$

where e_j results from (16), N=80000 is the number of records. The following numerical values of MSE were obtained: $\mathrm{MSE}_{PRBS} = 7.2096 \cdot 10^{-8}$, $\mathrm{MSE}_{STAIRS} = 3.5279 \cdot 10^{-8}$ in case of PRBS control input, $\mathrm{MSE}_{SINE} = 1.1904 \cdot 10^{-7}$ in case of sine control input, $\mathrm{MSE}_{CHIRP} = 1.8753 \cdot 10^{-8}$ in case of chirp control input and $\mathrm{MSE}_{PWM} = 8.9096 \cdot 10^{-8}$ in case of Pulse–width modulation (PWM) control input. The MSE numerical values are small because the ranges of stMaglev and TPmodel outputs are less than 10 mm.

The percent relative modeling errors have the following expressions:

$$e_{rj}[\%] = | e_j | / | y_{MLS_j} | \cdot 100. \tag{18}$$

The plot of the percent relative modeling errors in case of the PRBS control signal is illustrated in Figure 9. The plots of the percent relative modeling errors in all new testing scenarios are illustrated in Figures 10-13.

The large values of the percent relative modeling errors in the initial phase of system responses are caused by neglecting the fourth state variable of stMaglev, the bottom electromagnet current, in the design of stMaglev and next the derivation of TP-m.

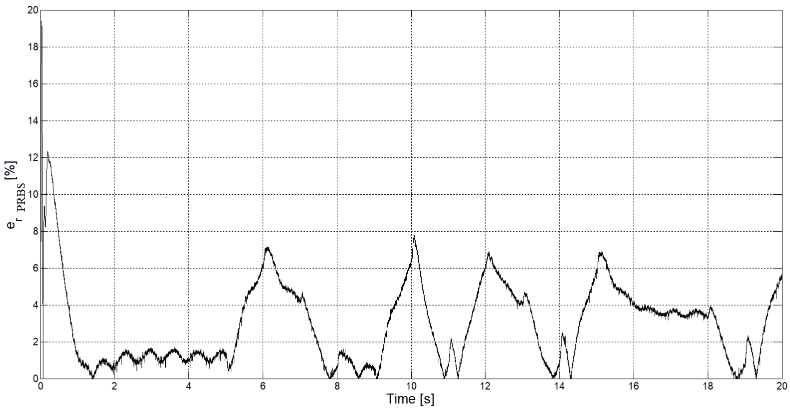

Figure 9

Percent relative modeling error with PRBS control input

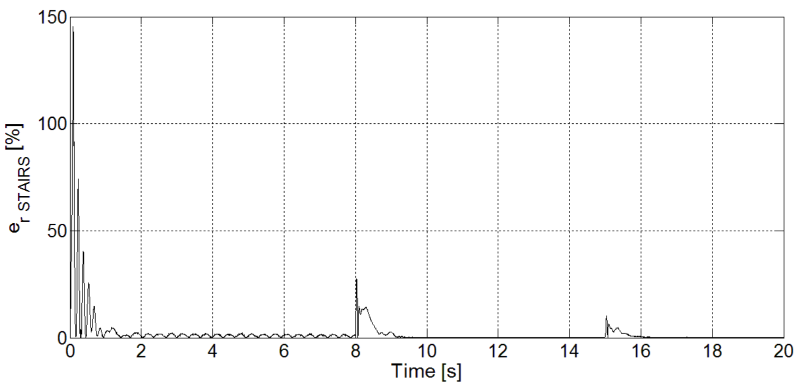

Figure 10

Percent relative modeling error with staircase control input

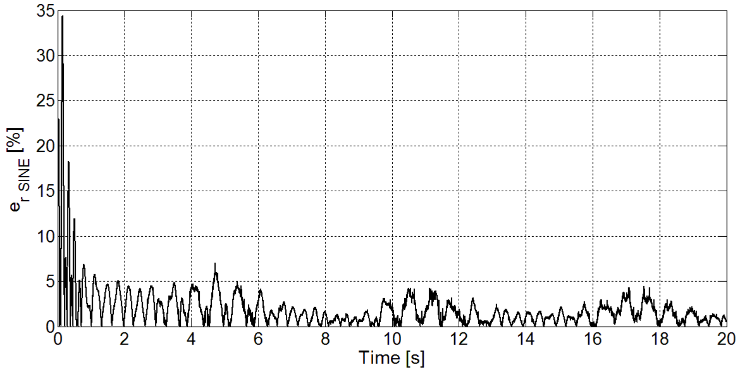

Figure 11
Percent relative modeling error with sine control input

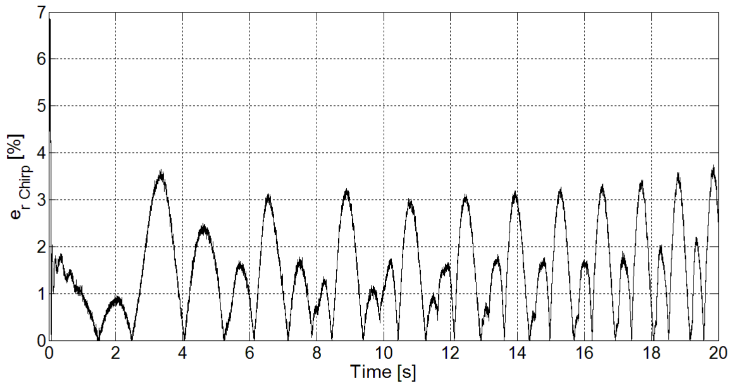

Figure 12
Percent relative modeling error with chirp control input

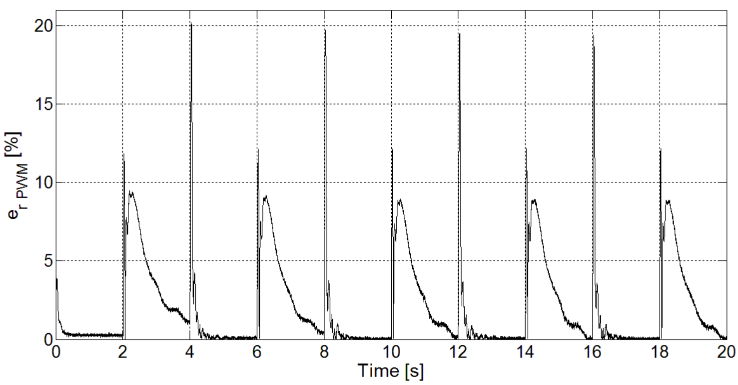

Figure 13
Percent relative modeling error with PWM control input

Conclusions

This paper proposed an extension of the ideas suggested in Hedrea et al. (2019) [17] by means of four new testing scenarios and adding useful information on the nonlinear plant that is subjected to the attractive nonlinear modeling and control technique built around TP. The new testing scenarios are important as a nonlinear plant is controlled and the TPmodel proposed by Hedrea et al. (2019) in [17] and this paper and will next be used in model-based control requires adequate validation. Various operating regimes were considered in this respect, and three performance indices, namely the modeling error, the mean square error and the percent relative modeling error, were also computed.

The experimental results show that the derived TPmodel approximates the behavior of the plant, but exhibiting a numerical approximation error which depends on the model parameters. The numerical values of the performance indices show that the TPmodel ensures good performance in terms of mean square error and percent relative modeling error in all testing scenarios, which are relevant to the real process operation. Experimental results also show that approximation errors are generally low, but depend on the control input.

Future research will be focused on finding what options are available to further reduce the approximation errors of the derived TPmodels or, in other words, to analyze what parameters do the approximation errors depend on. Future research will also include a part of the next directions already identified and proposed in (Hedrea et al., 2019) [17]: the derivation of other TPmodels for different plants, and the adaptation of results from other models and application areas. Such promising and also challenging plants and applications include robotics [28-31], fuzzy models and control [32-38], neural networks [39], medicine [40-42], servo systems and engines [43, 44], supervisory control [45], and various modern optimization algorithms [46-51] applied to controller tuning and system model identification as well.

Acknowledgement

This work was supported by Accenture, a grant of the Politehnica University of Timisoara, Romania, project number PCD-TC-UPT-2017, and the CNFIS-FDI-2019-0696 project of the Politehnica University of Timisoara, Romania.

References

[1] P. Baranyi: TP Model Transformation as a Way to LMI-based Controller Design, IEEE Transactions on Industrial Electronics, Vol. 51, No. 2, 2004, pp. 387-400

[2] Z. Petres, P. Baranyi, P. Korondi, H. Hashimoto: Trajectory Tracking by TP Model Transformation: Case Study of a benchMark Problem, IEEE Transactions on Industrial Electronics, Vol. 54, No. 3, 2007, pp. 1654-1663

[3] P. Baranyi, Y. Yam, P. Varlaki: TP Model Transformation in Polytopic Model-based Control. Boca Raton, FL: Taylor & Francis, 2013

[4] P. Korondi: Tensor Product Model Transformation-based Sliding Surface Design, Acta Polytechnica Hungarica, Vol. 3, No. 4, 2006, pp. 23-36

[5] P. Galambos, J. Kuti, P. Baranyi, G. Szögi, I. J. Rudas: Tensor Product-based Convex Polytopic Modeling of Nonlinear Insulin-Glucose Dynamics, in Proceedings of 2015 IEEE International Conference on Systems, Man and Cybernetics, Hong Kong, 2015, pp. 2597-2602

[6] E.-L. Hedrea, R.-E. Precup, C.-A. Bojan-Dragos, C. Hedrea: Tensor Product-based Model Transformation Technique Applied to Modeling Vertical Three Tank Systems, in Proceedings of the 12th IEEE International Symposium on Applied Computational Intelligence, Timisoara, Romania, 2018, pp. 63-68

[7] J. Kuti, P. Galambos: Tensor Product Model-based PID Controller Optimisation for Propofol Administration, IFAC-PapersOnLine, Vol. 51, No. 4, 2018, pp. 645-650

[8] P. Baranyi: TP-Model Transformation-Based-Control Design Frameworks. Cham: Springer International Publishing Switzerland, 2016

[9] A. Szöllösi, P. Baranyi: Influence of the tensor product model representation of qLPV models on the feasibility of linear matrix inequality, Asian Journal of Control, Vol. 18, No. 4, 2016, pp. 1328-1342

[10] A. Szöllösi, P. Baranyi: Influence of the tensor product model representation of qLPV models on the feasibility of linear matrix inequality based stability analysis, Asian Journal of Control, Vol. 20, No. 1, 2018, pp. 531-547

[11] P. Baranyi: Extension of the multi-TP model transformation to functions with different numbers of variables, Complexity, Vol. 2018, 2018, pp. 1-9

[12] P. Baranyi: Extracting LPV and qLPV structures from state-space functions: a TP model transformation based framework, IEEE Transactions on Fuzzy Systems, 2019, DOI: 10.1109/TFUZZ.2019.2908770

[13] J. J. Rubio, L. Zhang, E. Lughofer, P. Cruz, A. Alsaedi, T. Hayat: Modeling and control with neural networks for a magnetic levitation system, Neurocomputing, Vol. 227, 2017, pp. 113-121

[14] R.-E. Precup, C.-A. Bojan-Dragos, E.-L. Hedrea, M.-D. Rarinca, E. M. Petriu: Evolving fuzzy models for the position control of magnetic levitation systems, in Proceedings of 2017 IEEE Conference on Evolving and Adaptive Intelligent Systems, Ljubljana, Slovenia, 2017, pp. 1-6

[15] Y. Sun, W. Li, J. Xu, H. Quiang, C. Chen: Nonlinear dynamic modeling and fuzzy sliding-mode controlling of electromagnetic levitation system of

low-speed maglev train, Journal of Vibroengineering, Vol. 19, No. 1, 2017, pp. 329-342

[16] R.-E. Precup, S. Preitl, C.-A. Bojan-Dragos, M.-B. Radac, A.-I. Szedlak-Stinean, E.-L. Hedrea, R.-C. Roman: Automotive applications of evolving Takagi-Sugeno-Kang fuzzy models, Facta Universitatis, Series: Mechanical Engineering, Vol. 15, No. 2, 2017, pp. 231-244

[17] E.-L. Hedrea, R.-E. Precup, C.-A. Bojan-Dragos, O. Tanasoiu: Tensor product-based model transformation technique applied to modeling magnetic levitation systems, in Proceedings of the 23rd IEEE International Conference on Intelligent Engineering Systems, Gödöllő, Hungary, 2019, pp. 179-184

[18] Inteco Ltd., Magnetic Levitation System 2EM (MLS2EM), User's Manual (Laboratory Set) Krakow, Poland: Inteco Ltd., 2008

[19] C.-A. Bojan-Dragos, M.-B. Radac, R.-E. Precup, E.-L. Hedrea, O.-M. Tanasoiu: Gain-Scheduling Control Solutions for Magnetic Levitation Systems, Acta Polytechnica Hungarica, Vol. 15, No. 5, 2018, pp. 89-108

[20] C. Pozna, R.-E. Precup, J. K. Tar, I. Škrjanc, S. Preitl: New results in modelling derived from Bayesian filtering, Knowledge-based Systems, Vol. 23, No. 2, 2010, pp. 182-194

[21] T. Haidegger, L. Kovács, S. Preitl, R.-E. Precup, B. Benyó, Z. Benyó: Controller design solutions for long distance telesurgical applications, International Journal of Artificial Intelligence, Vol. 6, No. S11, 2011, pp. 48-71

[22] R.-E. Precup, M. L. Tomescu, S. Preitl, E. M. Petriu, J. Fodor, C. Pozna: Stability analysis and design of a class of MIMO fuzzy control systems, Journal of Intelligent and Fuzzy Systems, Vol. 25, No. 1, 2013, pp. 145-155

[23] Á. Takács, L. Kovács, I. Rudas, R.-E. Precup, T. Haidegger: Models for Force Control in Telesurgical Robot Systems, Acta Polytechnica Hungarica, Vol. 12, No. 8, 2015, pp. 95-114

[24] Z. Petres: Polytopic Decomposition of Linear Parameter-Varying Models by Tensor-Product Model Transformation, PhD Thesis, Budapest University of Technology and Economics, Budapest, Hungary, 2006

[25] L. Lathauwer, B. De Moor, J. Vandewalle: A multilinear singular value decomposition, SIAM Journal of Matrix Analysis and Applications, Vol. 21, No. 4, 2000, pp. 1253-1278

[26] E.-L. Hedrea, C.-A. Bojan-Dragos, R.-E. Precup, R.-C. Roman, E. M. Petriu, C. Hedrea: Tensor product-based model transformation for position control of magnetic levitation systems, in Proceedings of 26th International Symposium on Industrial Electronics, Edinburgh, UK, 2017, pp. 1-6

[27] S. Nagy, Z. Petres, P. Baranyi: TP Tool – A Matlab Toolbox for TP Model Transformation, in Proceedings of 8th International Symposium on Computational Intelligence and Informatics, Budapest, Hungary, 2007, pp. 483-495

[28] J. Vaščák, M. Rutrich: Path planning in dynamic environment using fuzzy cognitive maps, in Proceedings of 6th International Symposium on Applied Machine Intelligence and Informatics, Herľany, Slovakia, 2008, pp. 5-9

[29] S. Blažič: On periodic control laws for mobile robots, IEEE Transactions on Industrial Electronics, Vol. 61, No. 7, 2014, pp. 3660-3670

[30] B. Kovács, G. Szayer, F. Tajti, M. Burdelis, P. Korondi: A novel potential field method for path planning of mobile robots by adapting animal motion attributes, Robotics and Autonomous Systems, Vol. 82, 2016, pp. 24-34

[31] C. Pozna, R.-E. Precup: An approach to the design of nonlinear state-space control systems, Studies in Informatics and Control, Vol. 27, No. 1, 2018, pp. 5-14

[32] R.-E. Precup, S. Preitl: Popov-type stability analysis method for fuzzy control systems, in Proceedings of Fifth European Congress on Intelligent Technologies and Soft Computing (EUFIT'97), Aachen, Germany, 1997, Vol. 2, pp. 1306-1310

[33] R.-E. Precup, S. Preitl: Fuzzy Controllers. Timisoara: Editura Orizonturi Universitare, 1999

[34] P. Angelov, N. Kasabov: Evolving computational intelligence systems, in Proceedings of 1st International Workshop on Genetic Fuzzy Systems, Granada, Spain, 2005, pp. 76-82

[35] Zs. Cs. Johanyák: A simple fuzzy logic based power control for a series hybrid electric vehicle, in Proceedings of 9th IEEE European Modelling Symposium, Madrid, Spain, 2015, pp. 207-212

[36] I. Dzitac, F. G. Filip, M. J. Manolescu: Fuzzy logic is not fuzzy: World-renowned computer scientist Lotfi A. Zadeh, International Journal on Computers Communications and Control, Vol. 12, No. 6, 2017, pp. 748-789

[37] F. Olivas, F. Valdez, O. Castillo, C. I. González, G. E. Martinez, P. Melin: Ant colony optimization with dynamic parameter adaptation based on interval type-2 fuzzy logic systems, Applied Soft Computing, Vol. 53, 2017, pp. 74-87

[38] V. Nikolić, M. Milovančević, D. Petković, D. Jocić, M. Savić: Parameters forecasting of laser welding by the artificial intelligence techniques, Facta Universitatis, Series: Mechanical Engineering, Vol. 18, No. 2, 2018, pp. 193-201

[39] I. Dumitrache, N. Constantin, M. Drăgoicea: Retele neurale: identificarea si conducerea proceselor. Bucharest: Matrix Rom, 1999

[40] H. Costin, C. Rotariu: Medical image analysis and representation using a fuzzy and rule-based hybrid approach, International Journal on Computers Communications and Control, Vol. 1, No. S, 2006, pp. 156-162

[41] L. Kovács: Linear Parameter Varying (LPV) based robust control of type-I diabetes driven for real patient data, Knowledge-Based Systems, Vol. 122, 2017, pp. 199-213

[42] R.-E. Precup, T.-A. Teban, A. Albu, A.-I. Szedlak-Stinean, C.-A. Bojan-Dragos: Experiments in incremental online identification of fuzzy models of finger dynamics, Romanian Journal on Information Science and Technology, Vol. 21, No. 4, 2018, pp. 358-376

[43] R.-E. Precup, S. Preitl: Development of fuzzy controllers with non-homogeneous dynamics for integral-type plants, Electrical Engineering, Vol. 85, No. 3, 2003, pp. 155-168

[44] R. Andoga, L. Főző, J. Judičák, R. Bréda, S. Szabo, R. Rozenberg, M. Džunda: Intelligent situational control of small turbojet engines, International Journal of Aerospace Engineering, Vol. 2018, article ID 8328792, 2018, pp. 1-16

[45] R. E. Haber, J. R. Alique, S. Ros Torrecillas, C. R. Peres Ferreira: Fuzzy supervisory control of end milling process, Information Sciences, Vol. 89, No. 1, 1996, pp. 95-106

[46] B. Niu, Y., Fan, H. Wang, L. Li, X. Wang: Novel bacterial foraging optimization with time-varying chemotaxis step, International Journal of Artifficial Intelligence, Vol. 7, No. A11, 2011, pp. 257-273

[47] R.-E. Precup, M.-L. Tomescu, C.-A. Dragos: Stabilization of Rössler chaotic dynamical system using fuzzy logic control algorithm, International Journal of General Systems, Vol. 43, No. 5, 2014, pp. 413-433

[48] T. V. Tran, Y. N. Wang: Artificial chemical reaction optimization algorithm and neural network based adaptive control for robot manipulator, Control Engineering and Applied Informatics, Vol. 19, No. 2, 2017, pp. 61-70

[49] M. Shams, E. Rashedi, S. M. Dashti, A. Hakimi: Ideal gas optimization algorithm, International Journal of Artifficial Intelligence, Vol. 15, No. 2, 2017, pp. 116-130

[50] S. Vrkalovic, E.-C. Lunca, I.-D. Borlea: Model-free sliding mode and fuzzy controllers for reverse osmosis desalination plants, International Journal of Artifficial Intelligence, Vol. 16, No. 2, 2018, pp. 208-222

[51] E. Osaba, X. S. Yang, I. Fister Jr, J. Del Ser, P. Lopez-Garcia, A. J. Vazquez-Pardavila: A discrete and improved bat algorithm for solving a medical goods distribution problem with pharmacological waste collection, Swarm and Evolutionary Computation, Vol. 44, 2019, pp. 273-286